SELECTIVITY, SPECIFICITY, AND SENSITIVITY IN THE PHOTOIONIZATION OF SPUTTERED SPECIES*

D.M. Gruen, W.F. Calaway, M.J. Pellin, C.E. Young
Materials Science/Chemistry/Chemical Technology Divisions
Argonne National Laboratory
Argonne, IL

D.R. Spiegel, R.N. Clayton, A.M. Davis
Department of Geophysical Sciences
University of Chicago
Chicago, IL

J. D. Blum
Department of Earth Sciences
Dartmouth College
Hanover, NH

CONF-9009327--1

DE91 006568

To be presented at:

8th International Workshop on
Inelastic Ion Surface Collisions Conference
Vienna, Austria

September 17-21, 1990

---

*Work supported in part through the U.S. Department of Energy, BES-Materials Sciences, under Contract W-31-109-ENG-38 to Argonne; BES-Engineering and Geosciences Grant DE-FG03-88ER13851 to Caltech; and through NASA Grants NAG9-51 and NAG9-111.

SELECTIVITY, SPECIFICITY, AND SENSITIVITY IN THE PHOTOIONIZATION OF SPUTTERED SPECIES

D.M. Gruen, M.J. Pellin, C.E. Young, W.F. Calaway
Materials Science/Chemistry/Chemical Technology Divisions
Argonne National Laboratory
Argonne, IL

D.R. Spiegel, R.N. Clayton, A.M. Davis
Department of Geophysical Sciences
University of Chicago
Chicago, IL

J. D. Blum
Department of Earth Sciences
Dartmouth College
Hanover, NH

Introduction

Resonance ionization of sputtered species has emerged as an exceedingly powerful technique for surface compositional analysis and as a means to study a variety of fundamental aspects of the sputtering process [1]. As examples of the latter application, one may mention studies of the depth of origin of sputtered species [2], their angular distributions, and the dependence of the sputtering yield on ion fluence in the 10^{12} - 10^{15} ions/cm^2 regime [3]. The technique is now being developed for measuring isotope ratios with particular application to problems in the geo- and planetary sciences [4-7]. The aim of much of the Argonne work has been to design instrumentation in such a way as to maximize sensitivity for the particular atomic or molecular species to be detected. A measure of detection sensitivity is the useful yield defined as the number of atoms (or molecules) detected per atom (or molecule) sputtered. Quantities that enter the useful yield expression include, for example, the instrument transmission function and the photoionization efficiency of the species to be detected. The first of these quantities can be about 0.2, taking into account geometric collection efficiencies from the available laser ionization volume, while the second can approach unity [8].

Less attention has been given to "noise" sources which tend to degrade the usefulness of the measurements due to non- or near-resonantly ionized species that isobarically overlap the species of interest. The high-ionization efficiency of resonance laser radiation and its potentially high selectivity for specific, especially atomic, systems has overshadowed the fact that non- or near-resonant ionization of unwanted species frequently occurs to some extent and can become a troublesome problem either for trace analysis at the ppb level (e.g., Fe in Si) [9], or for isotope ratio determination (e.g., Ca and Ti), or for both (e.g., Os and Re) [4,5].

To deal with the problem of non- or near-resonant ionization, one needs to achieve the highest selectivity for photoionization of the species of interest relative to isobarically overlapping species by choosing a specific photoionization scheme tailored to that purpose. Two partial prescriptions for the proper choice of an optimal photoionization scheme are that it should not have near-overlap with known atomic or molecular energy levels of isobaric species, and that it should lead to saturation of the resonance transitions at the lowest possible laser power levels so as to minimize two- and three-photon nonresonant photoionization processes. Experience has shown that, even when these two conditions are met as closely as possible, non- or near-resonant ionization can still occur, perhaps because of the existence of hitherto unobserved energy levels, photodissociation of sputtered molecules, or other effects. It is becoming clear that maximizing detection sensitivity for a particular species requires one to pay careful attention to the selection of an optimal photoionization scheme. It is the purpose of the present paper to illustrate this point with several examples and to help point the way to still further improvements in detection sensitivity by minimizing non- or near-resonant ionization through detailed exploration of alternative photoionization schemes.

Results and Discussion

All results to be presented and discussed here were obtained on the SARISA IV instrument which was developed and has been operated at the Argonne National Laboratory. The design and performance characteristics of this instrument have been thoroughly documented in the literature and the reader is referred to the relevant papers [1,8].

A. Osmium and Rhenium

The Re-Os system is the only viable radiometric dating method for meteorites involving long-lived siderophile elements [10]. Current state of the art involves chemical separation of Re and Os from a bulk meteorite, measurement of Re and Os concentrations by isotope dilution and measurement of $^{187}Os/^{186}Os$. Most of the isotopic measurements have been made by SIMS on chemically separated Re and Os. It is essential to cleanly separate Re from Os since ^{187}Re and ^{187}Os have the same mass to within 1 part in 10^6 and, therefore, constitute very serious isobaric interferences. Chemical separation is very difficult to do consistently and limits precision of measurements of $^{187}Os/^{186}Os$ to $\pm$ 0.5 - 1% (2 σ) [11].

An additional problem with SIMS for Os and Re is that ion fractions are in the range 10^{-5} - 10^{-6}, and the technique, therefore, has very low sensitivity for these two elements.

Resonance ionization of sputtered Re and Os has recently been shown to be very selective and sensitive leading to a minimum detection limit of 7 ppb atomic and a useful yield of 1% for Os [4,5]. To achieve these results, Os was ionized by five different schemes shown in fig. 1 to evaluate their sensitivities and selectivities. Rhenium was ionized by schemes A and B in fig. 1. Scheme E was found to be most favorable for Os ionization and involves excitation to two resonance levels with a third ionizing photon generated from a dye laser tuned to reach an autoionizing resonant energy level above the ionization potential.

The *in situ* measurement of the isotopic composition of Os in samples that also contain Re requires that ^{187}Re ionization (62.6% isotopic abundance) be suppressed to eliminate isobaric interference with the ^{187}Os peak (~ 1.6% isotopic abundance). To show the selectivity of each Os^+ ionization scheme, the $^{192}Os^+/^{185}Re^+$ ratios are displayed in fig. 2. It can be seen that Os was enhanced relative to Re by as much as 33 by the single resonance scheme C, by a factor of 10^2 for the double resonance scheme D, and by $\leq 10^3$ for the triple resonance scheme E.

A convincing example of low versus high selectivity ionization schemes is shown in the next two figures. The time-of-flight mass spectra shown in fig. 4 were obtained using the specific ionization schemes for Re and Os, respectively, shown in fig. 3. The low selectivity of scheme B for Re is illustrated by the presence of nonresonantly ionized Os observed at masses 188 to 192 in fig. 4a. A similar spectrum is shown in fig. 4b for resonance ionization of Os from the same sample by ionization scheme E. The very high selectivity of scheme E for Os is illustrated by the complete absence of Re at mass 185 and 187.

B. Titanium and Calcium

It is now known that there are components of calcium-aluminum inclusions in meteorites that are enriched or depleted in the neutron-rich isotopes of Ca, Ti, Cr, Fe, Ni, and Zr. The sizes of anomalies in the neutron-rich isotopes of these elements provide important constraints on nucleosynthesis models for the iron peak such as the neutron-rich statistical equilibrium model [12]. We are now developing techniques to measure Ca and Ti isotope ratios *in situ* in meteoritic materials and as a first step are investigating the selective photoionization of Ti in the presence of Ca.

A SIMS spectrum obtained from a sample of perovskite of meteoritic origin is shown in fig. 5 with signal intensities displayed as the ordinate and plotted on a log scale. The mass range of interest, 35-65, is shown for the same perovskite sample in fig. 6 with the signal level (normalized to $^{48}Ti = 100$) on a linear scale. The first panel shows again the SIMS results replotted for the appropriate mass range from fig. 5. It can be seen that the Ca^+/Ti^+ ratio in SIMS is ≈ 10. Since the natural isotopic abundance of ^{48}Ca is 0.18%, the very large Ca^+ signal in SIMS constitutes a serious isobaric interference preventing the accurate determination of Ti isotope ratios.

Two photoionization schemes (labeled scheme 1 and scheme 2 in fig. 7) have been investigated for Ti. Both schemes involve, as in scheme E for Os, three resonance steps with the third ionizing photon tuned to an autoionizing level above the ionization potential. Both Ti ionization schemes originate in the ground $^3Fe_2$ state of the neutral Ti atom and use the $^3F_3$ state at 19,421 cm^{-1} as

the first resonant step. The two schemes differ primarily in the second resonant level which is the g $^3F_3$ state at 41,988 cm^{-1} for scheme 1 and the e $^3F_3$ state at the 37,660 cm^{-1} for scheme 2. The effects of using the two schemes on Ca^+/Ti^+ ratios are dramatic. For scheme 1, the Ca^+/Ti^+ ratio is ≈ 0.2 (panel 2) and for scheme 2, it is ≈ 0.01 (see panel 3, fig. 6). Compared to SIMS then, scheme 2 represents a factor 10^3 selectivity for Ti compared to Ca ionization. Thus, in principle, Ti ratios can now be determined even in the presence of Ca by using scheme 2 for Ti photoionization.

Furthermore, fig. 6 shows no mass peaks at mass 56 (CaO,Fe) for photoionization whereas these peaks are prominent in the SIMS spectrum. On the other hand, TiO is observed in SIMS as well as in the photoionization spectrum albeit somewhat reduced for scheme 2 ionization.

C. Fe in Si

In secondary neutral mass spectrometry (SNMS), the major sputtered species from most materials are neutral atoms. Thus, detection of trace amounts of material requires highly efficient ionization of the neutral species. Matrix effects in the sputtered neutral flux are usually minor so quantitative analysis of trace species can be performed fairly readily using SNMS. It has been shown that for single element analysis, resonant ionization mass spectrometry (RIMS) can be a very sensitive form of SNMS,[13-15] the major advantages being ease of complete ionization of the neutrals and discrimination of isobaric interfering species as described in the present paper.

Much of the RIMS work done at Argonne has accentuated the design of the mass spectrometer as the key to improving signal to noise and thus detection sensitivity. In this paper, however, we wish to emphasize the role of spectroscopy in improving sensitivity. This can be accomplished either by identifying more efficient ionization paths or by reducing noise produced by nonresonant ionization. In a RIMS experiment, noise is contributed by any ion detected at the mass of interest which does not originate from resonant ionization of the species of interest. Ions scattered during the sputtering process, sputtered secondary ions, and nonresonantly ionized species, either the same or different from the element of interest, are noise sources. Further,

the detection limit of the experiment is dependent upon the magnitude of the background level which can be attained. For fixed instrument transmission when complete ionization occurs, reduction of background noise is the only way to improve the detection limit of the instrument.

With the particular RIMS instrument developed at Argonne, surface analysis by resonance ionization of sputtered atoms (SARISA), virtually all stray ions and sputtered secondary ions have been eliminated as noise sources leaving only nonresonant ionized species to contend with. Thus, to improve sensitivity in SARISA, it is important to choose an ionization scheme that completely ionizes the species of interest and yet minimizes the nonresonant ionization of that species as well as any isobaric interfering species.

Another pertinent example is Fe in Si. We have investigated the three different ionization schemes for Fe portrayed in fig. 8. The first scheme employs three-color, 1+1+1 ionization where two resonant levels as well as an autoionizing level are accessed via tunable dye lasers. The other two schemes employ two-color, 1+1 ionization that access different intermediate energy levels via a tunable dye laser but use the same fix frequency XeCl excimer laser (308 nm) to ionize Fe. As reported earlier [16], the two-color ionization scheme on the righthand side of fig. 8 produces a small amount of nonresonant Fe^+ (~ 1% of the resonant signal) and a substantial amount of Si_2^+ (0.12 counts/ pulse). The Si_2^+ background restricts the detection limit for Fe in Si to about 2 ppb for this ionization scheme. The other two-color scheme behaves similarly. This is not surprising since both resonant transitions were easily saturated at relatively low laser intensities and the 308 nm excimer radiation generates most of the Si_2^+. By going to an ionization scheme that employs three colors to ionize Fe, the Si_2^+ background was reduced by almost a factor of 100 (0.0017 counts/pulse) with a corresponding increase of nearly 10 in sensitivity. Figure 9 shows the detection limit observed for SARISA employing both the two and three color ionization scheme as a function of number of laser shots.

A unique advantage of RIMS over other SNMS techniques is that background subtractions are easily accomplished in order to reduce noise. Since the species being monitored is detected only if a laser is tuned to a

resonance frequency for that species coupled to the ionization continuum, the background level can be determined simply by tuning the laser off the resonance frequency. Thus, ions striking the detector can be identified as signal or noise by scanning through an absorption band. By recording signal levels on and off the resonance frequency and then subtracting one from the other, interfering species can be discriminated against.

Figure 10 shows a mass spectrum of Fe in Si averaged over 160000 laser pulses obtained by resonantly ionizing Fe using the three-color scheme. The sample was fabricated by Siemens Corporation and has a nominal Fe concentration of 2 ppb as measured by deep-level transient spectroscopy (DLTS). Note that the mass spectrum shows substantial signals at masses 28 (Si), 39 (K), and 47 (SiF) in addition to a small signal at mass 56 (Fe + Si_2). When the frequency of the first resonance step is detuned and data is collected, the mass spectrum appears qualitatively the same. Subtracting the two spectra yields a signal only at mass 56. This confirms that all other features in the mass spectrum are produced by nonresonant ionization. The difference spectrum yields the Fe in Si signal for this sample and is shown in fig. 11. By integrating the signal about mass 56, a signal level of 0.0023 counts/pulse is obtained for this 2 ppb sample. From the signal and background count rates, it is possible to calculate the selectivity of Fe over Si_2. Assuming that all the noise counts are Si_2 and that at least 1% of the Si sputtered flux is dimer, it is estimated that the three-color ionization scheme enhances the Fe signal over the Si_2 signal by a factor of 10^6.

D. Fe in the Presence of Cr and Ni

Because of the success of the three-color ionization scheme to discriminate Fe from Si_2, the same ionization path has been chosen to examine the selective ionization of Fe in the presence of other iron group elements. To study problems in stellar nucleosynthesis, several isotopes of these elements would be of interest, were it not for difficulties in their analyses due to isobaric overlaps. Two examples are the isobaric interferences in the Fe/Cr system at mass 54 and in the Fe/Ni system at mass 58. The selectivity of the three-color ionization scheme for these isobars has been examined in the SARISA

apparatus using a foil of Inconel 600. The major constituents of this alloy are Ni (71 at.%), Cr (17 at.%), Fe (8 at.%), and Co (4 at.%).

A preliminary analysis of the Inconel sample by SIMS, obtained with the same energy and angular refocusing time-of-flight (EARTOF) mass spectrometer as is used with SARISA, confirmed the presence of the three elements of interest. The spectrum is shown in fig. 12. The relative intensities of the peaks for the different elements are the qualitatively expected ones based on their concentrations and ionization potentials. A RIMS mass spectrum of the same sample obtained with the SARISA instrument is shown in fig. 13. The same three-color ionization scheme that was employed for the Fe in Si analysis was again used. As expected, the predominant peak in the spectrum is Fe at mass 56. The isotopes of Fe at masses 54 and 57 are also present and are at approximately the correct intensity ratios when compared to mass 56. In addition, there are substantial signals due to nonresonantly ionized Ni at masses 58 and 60 as well as a small amount of Cr at mass 52. This is confirmed by tuning off the 344 nm Fe resonance as shown in fig. 14. From the concentrations of the three elements, the Fe selectivity is calculated to be 180 and 60 for Cr and Ni, respectively.

The situation for accurate isotope ratio determinations depends not only on the selectivity but also on the isotopic abundances. Since the isotopic abundance of ^{58}Ni is 0.6788 and that of ^{58}Fe is 0.0033, a selectivity of > 200 is needed just to detect equal quantities of Fe and Ni at mass 58. The selectivity of the three-color ionization scheme falls far short of even this minimum capability. An equivalent way of examining the selectivity would be to compare relative nonresonant ionization intensities, taking into account both concentration differences and isotope distributions. The calculated nonresonant ionization signal intensity ratio for Ni to Fe to Cr is 417:133:13, respectively. It is interesting to note that Cr, which has the largest SIMS signal, has the lowest nonresonant ionization signal and thus will be the easiest to discriminate against.

It is not clear why selectivity in the Fe/Ni system is so poor. Atomic transitions are very narrow and no known coincidence between those of Fe and Ni at the wavelengths employed are known. In addition, as can be seen from figs. 13

and 14, tuning the laser frequency off resonance from the 344 nm Fe transitions did not significantly affect the Ni intensity. This is also true for the other two frequencies used in the ionization scheme, thus demonstrating that only nonresonant processes are involved in the Ni ionization. In order better to understand the observed results, the intensity of the Fe, Ni, and Cr signals were recorded as the three lasers frequencies were incrementally turned on. Results of this study are shown in fig. 15 along with a comparison to the SIMS intensities. As can be seen from the data, Ni is ionized by both 344 nm and 510 nm photons. Only 640 nm light is ineffective in the ionization of Ni. On the other hand, very little Cr is ionized at any of these frequencies.

It appears that multiphoton ionization of ground state neutral Ni is not the mechanism for the observed Ni signal. The appropriate power dependence studies of the ionization process are yet to be completed. However, the intensities of the laser beams ($< 100\ mJ/cm^2$) are unlikely to cause substantial amounts of ionization unless near-resonant enhancements are occurring. We are unaware of Ni absorption bands near 344 nm and 510 nm which could produce such an enhancement. It seems possible that a more exotic ionization path is at work for Ni. This conclusion is also supported by the fact that the nonresonant Ni signal is significantly larger than either the Fe or Cr signals. In this regard, we are exploring the prospect that excited states of Ni or Ni containing molecules are involved in the ionization process. For instance, if a mechanism existed whereby Ni^+ could be efficiently produced from Ni_2 by photodissociation, it is estimated that about 5% of the total Ni flux would need to be in the form of dimers in order to produce the observed signal. It appears that this, or some similar process, may turn out to be the source of the nonresonantly ionized Ni and that the key to understanding the nonresonant ionization of Ni is better knowledge of the sputtering process and of the spectroscopy of Ni species.

Acknowledgement

Work supported in part through the U.S. Department of Energy, BES-Materials Sciences, under Contract W-31-109-ENG-38 to Argonne; BES-Engineering and Geosciences Grant DE-FG03-88ER13851 to Caltech; and

through NASA Grants NAG9-51 and NAG9-111. We would like to thank Dr. H. J. Zeininger of Siemens AG for preparing the Fe in Si sample.

References

[1] D. M. Gruen, M. J. Pellin, W. F. Calaway, and C. E. Young, Proceedings of SIMS VI, (A. Benninghoven, A. M. Huber, and H. W. Werner, Editors), Wiley, New York, 1988, pp. 789-796.

[2] J. W. Burnett, J. P. Biersack, D. M. Gruen, B. Jørgensen, A. R. Krauss, M. J. Pellin, E. L. Schweitzer, J. T. Yates, Jr., and C. E. Young, J. Vac. Sci. Techn. **A6**(3), 2064 (1988).

[3] J. W. Burnett, M. J. Pellin, W. F. Calaway, D. M. Gruen, and J. T. Yates, Jr., Phys. Rev. Lett. **63**, 562 (1989).

[4] J. D. Blum, M. J. Pellin, W. F. Calaway, C. E. Young, D. M. Gruen, I. D. Hutcheon, and G. J. Wasserburg, Anal. Chem. **62**, 2090 (1990).

[5] J. D. Blum, M. J. Pellin, W. F. Calaway, C. E. Young, D. M. Gruen, I. D. Hutcheon, and G. J. Wasserburg, (Geochim. Cosmochim. Acta **54**, 875 (1990).

[6] R. J. Walker, S. B. Shirey, and O. Stecher, Earth Planet. Sci. Lett. **87**, 1 (1988).

[7] N. Thonnard, R. D. Willis, M. C. Wright, and W. A. Davis, Nucl. Instr. Meth. Phys. Res. **B29**, 398 (1987).

[8] M. J. Pellin, C. E. Young, and D. M. Gruen, Scanning Microscopy **2**, 1353 (1988).

[9] C. E. Young, M. J. Pellin, W. F. Calaway, J. W. Burnett, D. M. Gruen, H. J. Stein, and S. S. Tsao, "Resonance Ionization Spectroscopy 1988," Inst. Phys. Conf. Ser. No. 94, 205 (1988). T. B. Lucatosto and J. E. Parks, Editors. Institute of Physics, Bristol, England.

[10] D. D. Clayton, "Principles of Stellar Evolution and Nucleosynthesis," p. 591, McGraw-Hill Book Co., New York (1968); Astrophys. J. **139**, 637 (1964).

[11] J. M. Luck and C. J. Allègre, Nature **302**, 130 (1983).

[12] D. Hartmann, S. E. Woosley, and M. F. El Eid, Astrophys. J. **297**, 837 (1985).

[13] M. J. Pellin, C. E. Young, W. F. Calaway, J. W. Burnett, B. Jorgensen, E. L. Schweitzer, and D. M. Gruen, Nucl. Instr. and Meth. **B18** (1987) 446-451.

[14] D. L. Pappas, D. M. Hrubowchak, M. H. Ervin, and N. Winograd, Science **243** (1989) 64-66.

[15] H. F. Arlinghaus, N. Thonnard, and H. W. Schmitt, in: Microbeam Analysis - 1989, P. E. Russell, ed. (San Francisco Press, 1989) p. 180.

[16] C. E. Young, M. J. Pellin, W. F. Calaway, B. Jorgensen, E. L. Schweitzer, and D. M. Gruen, Nucl. Instr. and Meth. **B27** (1987) 119-129.

Figure Captions

Fig. 1 - Generalized ionization schemes evaluated for Os (A-E) and Re (A-B). Asterisks denote broad-ban excimer radiation.

Fig. 2 - Relative selectivity for Os over Re measured as the log of the ratio of the observed to the true $^{192}Os^{+}/^{185}Re^{+}$ ratio for the Os ionization schemes.

Fig. 3 - Specific ionization schemes used for Re and Os analyses.

Fig. 4 - (a) Re spectrum (scheme B) taken at low mass resolution (~250) and (b) Os spectrum (scheme E) taken at higher mass resolution (~400) in the same synthetic sample (2.3% Re; 2.5% Os). Labels indicate the masses of the Re (185 and 187) and Os (186 to 190 and 192) isotope peaks. Note that scheme B for Re has low selectivity and scheme E for Os has high selectivity.

Fig. 5 - SIMS spectrum tuned for maximum transmission of a perovskite sample taken from the Magnet Cove, AR meteorite.

Fig. 6 - Mass spectra of perovskite sample from Magnet Cove, AR meteorite. Left panel: SIMS tuned for maximum transmission; middle panel: RIMS using scheme 1 of fig. 7; right panel: RIMS using scheme 2 of fig. 7.

Fig. 7 - Titanium photoionization schemes 1 and 2.

Fig. 8 - Partial energy level diagram for Fe showing the three ionization schemes used in the Si analysis.

Fig. 9 - Calculated detection limit for Fe in Si as a function of the number of laser pulses for both a two- and three-color ionization scheme.

Fig. 10 - RIMS spectrum of a 2 ppb Fe in Si sample obtained using the three-color ionization scheme and the SARISA apparatus.

Fig. 11 - On resonance minus off resonance difference mass spectrum of a 2 ppb Fe in Si sample obtained using the three-color ionization scheme and the SARISA apparatus.

Fig. 12 - SIMS mass spectrum of Inconel 600 obtained using the EARTOF.

Fig. 13 - RIMS mass spectrum of Fe from an Inconel 600 sample using SARISA and the three-color ionization scheme.

Fig. 14 - Nonresonant ionization mass spectrum of Inconel 600. The spectrum was obtained in an identical manner to the RIMS Fe spectrum in Fig. 2 except that the first ionization step (344.06 nm) was tuned off resonance 0.1 nm.

Fig. 15 - The relative intensity of Fe, Ni, and Cr signals obtained from SIMS and RIMS. The one-color RIMS experiment used only 344 nm laser light; the two-color experiment used 344 and 640 nm light; and the three-color experiment used 344, 640, and 510 nm light.

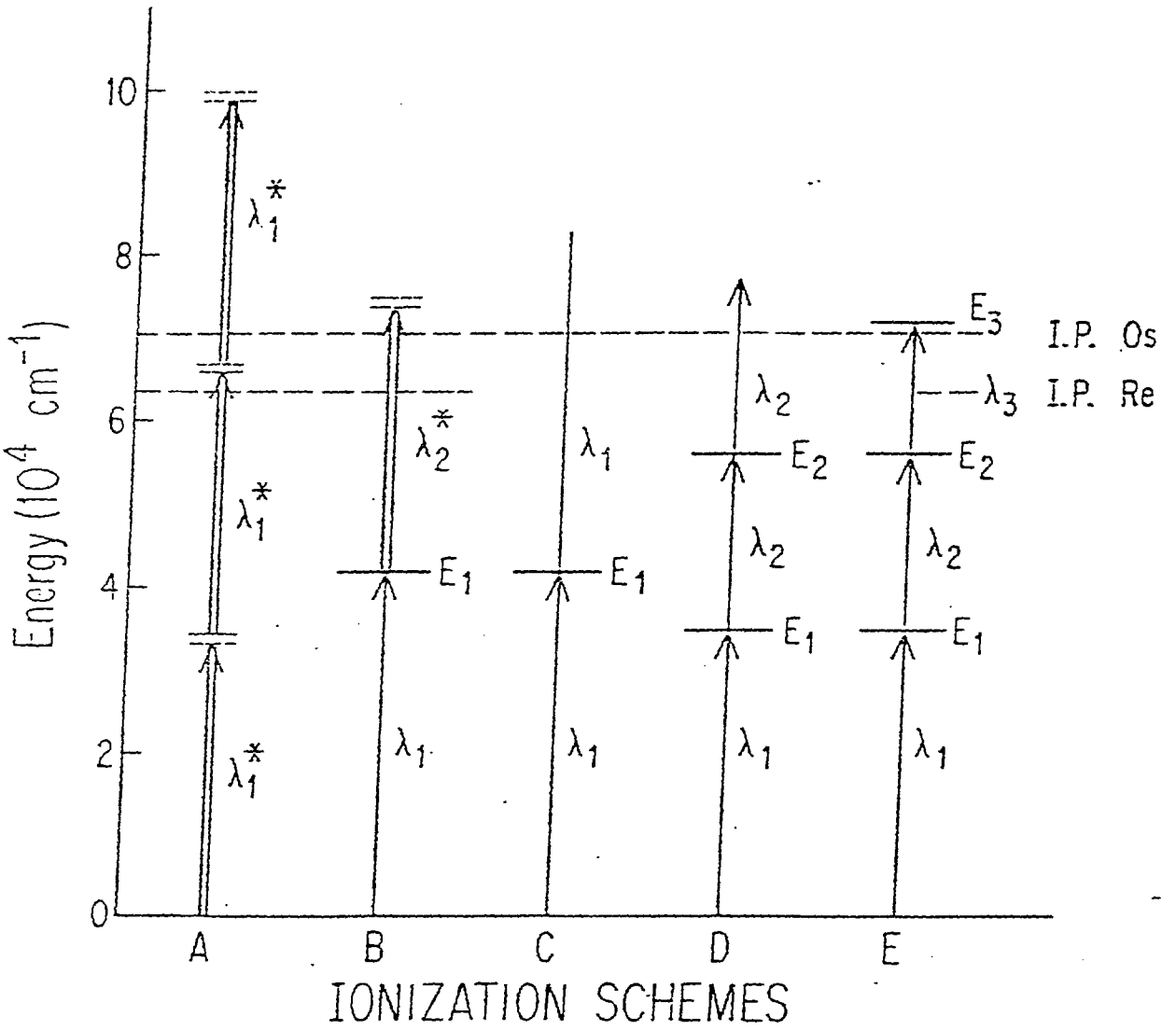
Energy (10^4 cm^{-1})
10
8
6
4
2
0
λ_1^*
λ_1^*
λ_1^*
λ_2^*
λ_1
λ_2
λ_2
λ_2
λ_3
E_3
E_2
E_2
E_2
E_1
E_1
E_1
E_1
λ_1
λ_1
λ_1
λ_1
I.P. Os
I.P. Re
A
B
C
D
E
IONIZATION SCHEMES

Fig. 1

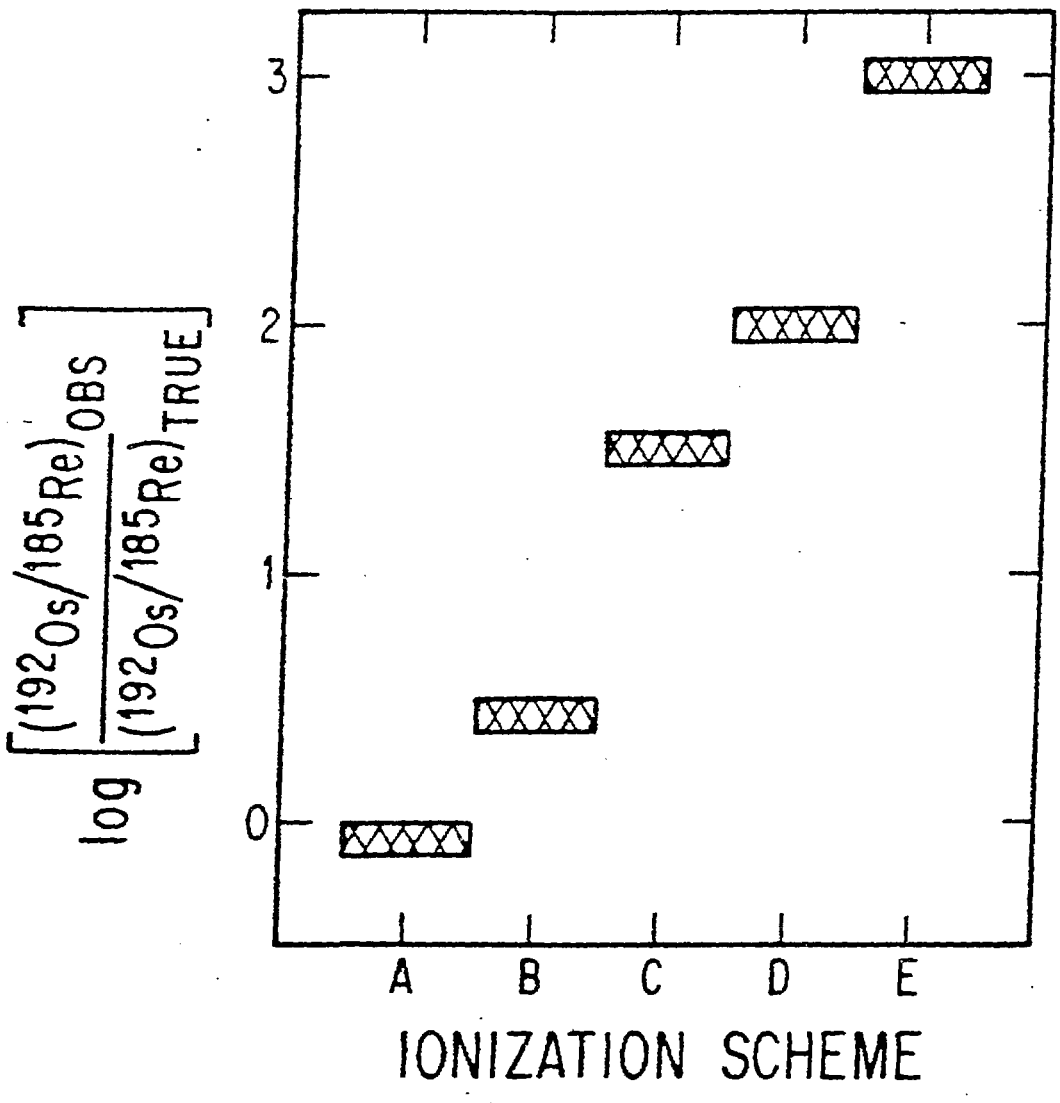
log [(192Os/185Re)OBS / (192Os/185Re)TRUE]
3
2
1
0
A
B
C
D
E
IONIZATION SCHEME

Fig. 2

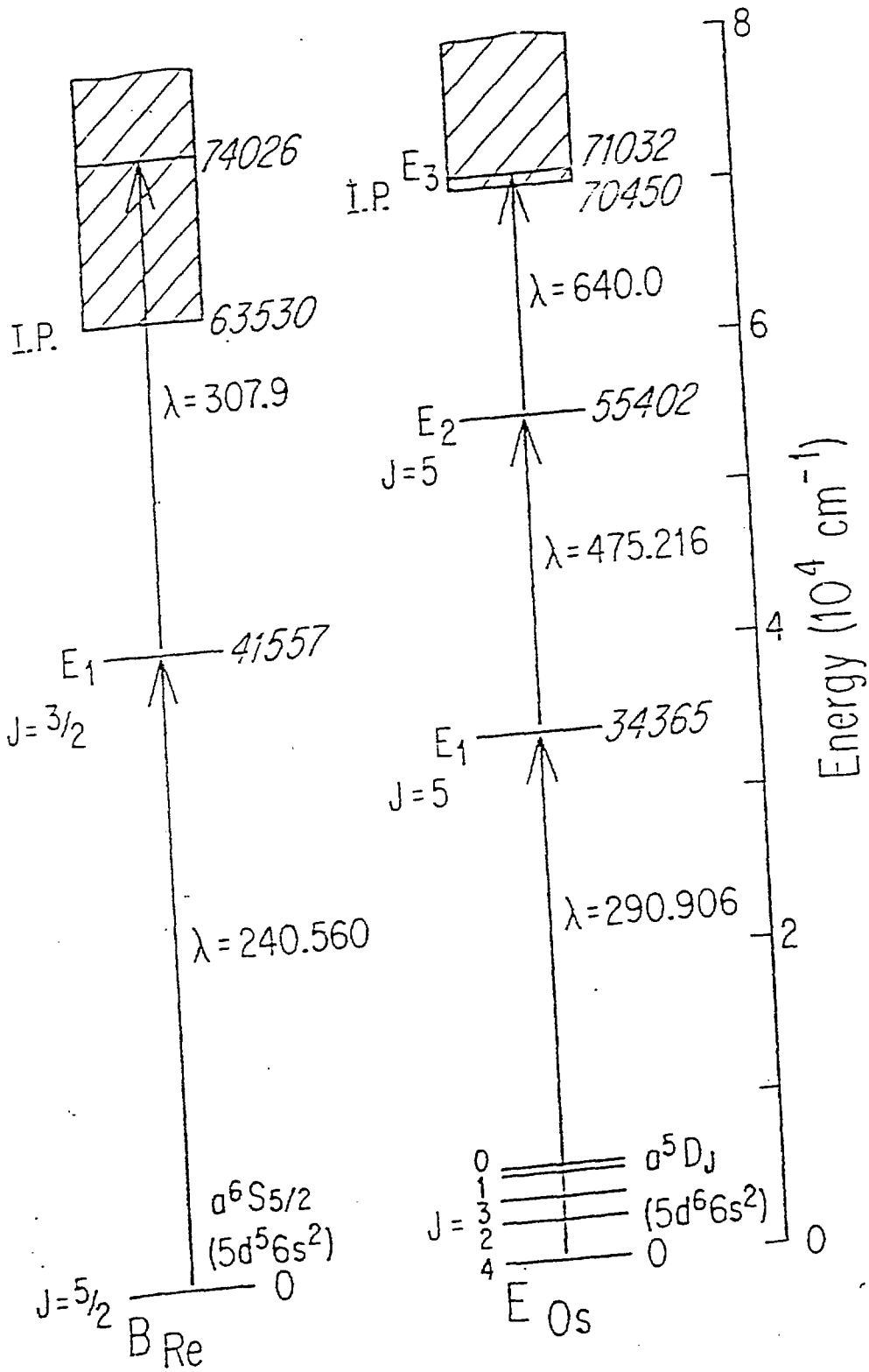
74026
I.P.
63530
λ = 307.9
E1
41557
J = 3/2
λ = 240.560
a6S5/2
(5d56s2)
J = 5/2
0
B Re
I.P.
E3
71032
70450
λ = 640.0
E2
55402
J = 5
λ = 475.216
E1
34365
J = 5
λ = 290.906
0
1
3
2
4
J =
a5DJ
(5d66s2)
0
E Os
8
6
4
2
0
Energy (10^4 cm^-1)

Fig. 3

Three Color RIMS of Os and Re
from a Synthetic Sample
(2.3% Re; 2.5% Os)

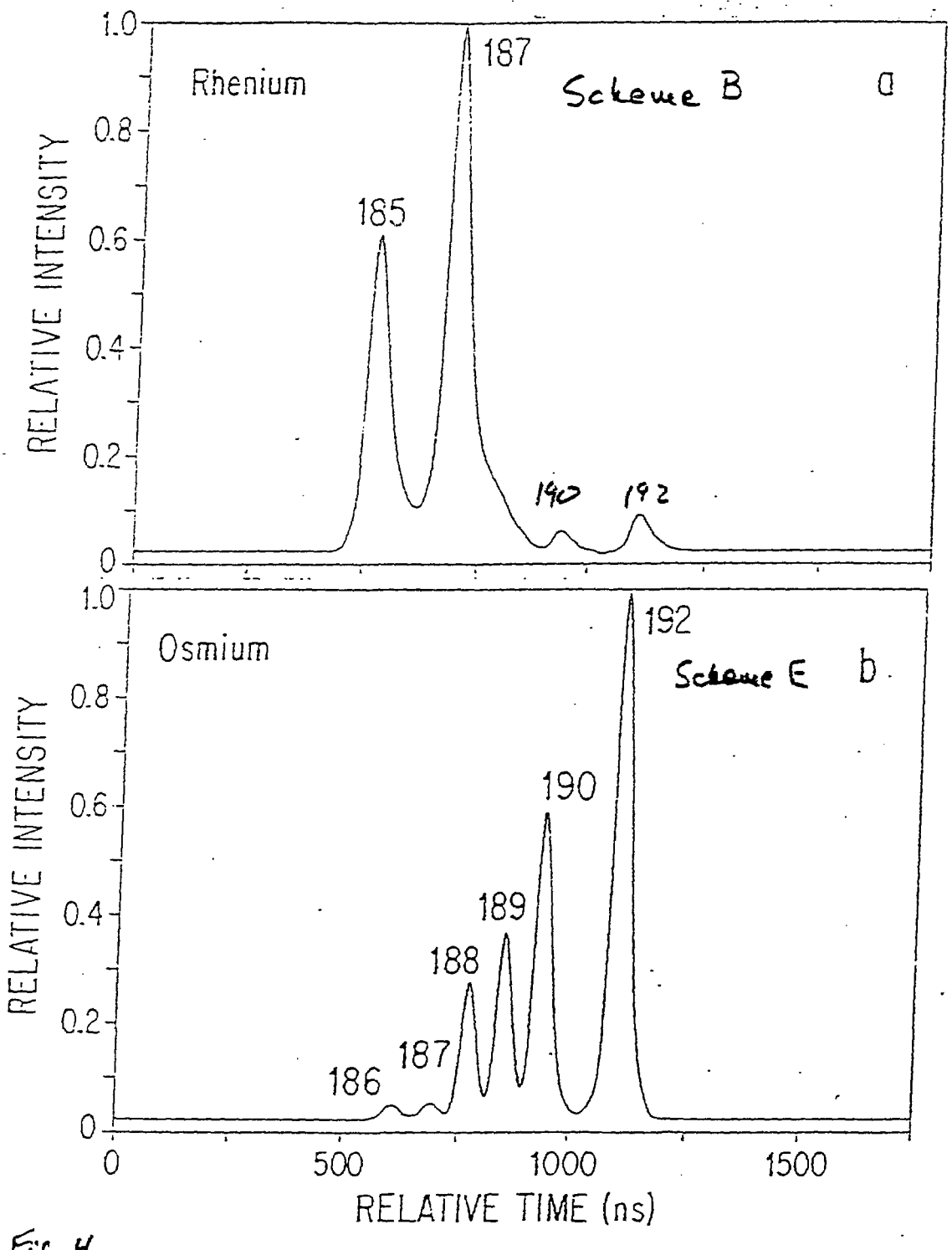

Fig. 4

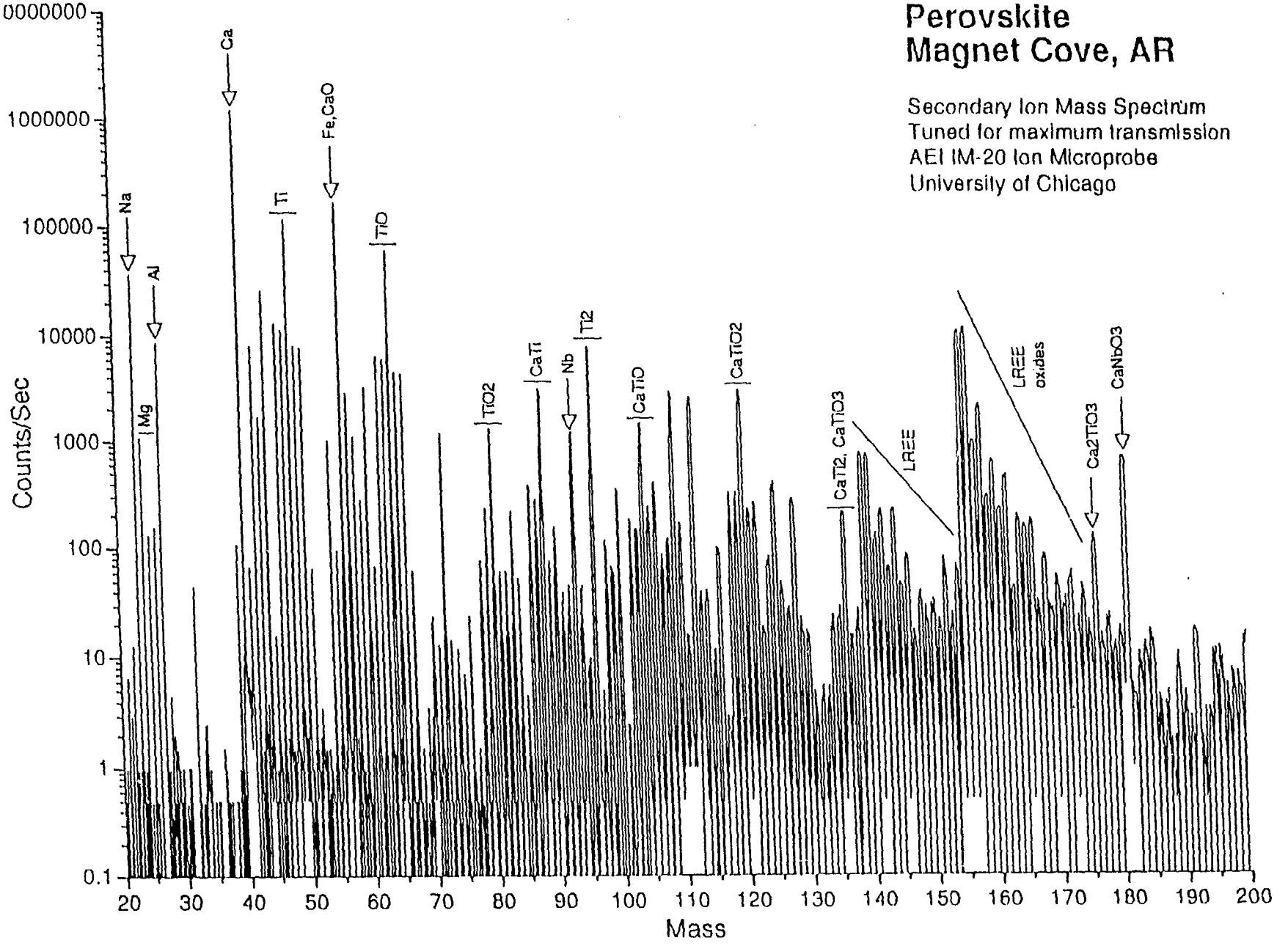
Perovskite
Magnet Cove, AR
Secondary Ion Mass Spectrum
Tuned for maximum transmission
AEI IM-20 Ion Microprobe
University of Chicago
Counts/Sec
Mass
10000000
1000000
100000
10000
1000
100
10
1
0.1
20
30
40
50
60
70
80
90
100
110
120
130
140
150
160
170
180
190
200
Na
Mg
Al
Ca
Ti
Fe,CaO
TiO
TiO2
CaTi
Nb
Ti2
CaTiO
CaTiO2
CaTi2, CaTiO3
LREE
LREE oxides
Ca2TiO3
CaNbO3

Fig. 5

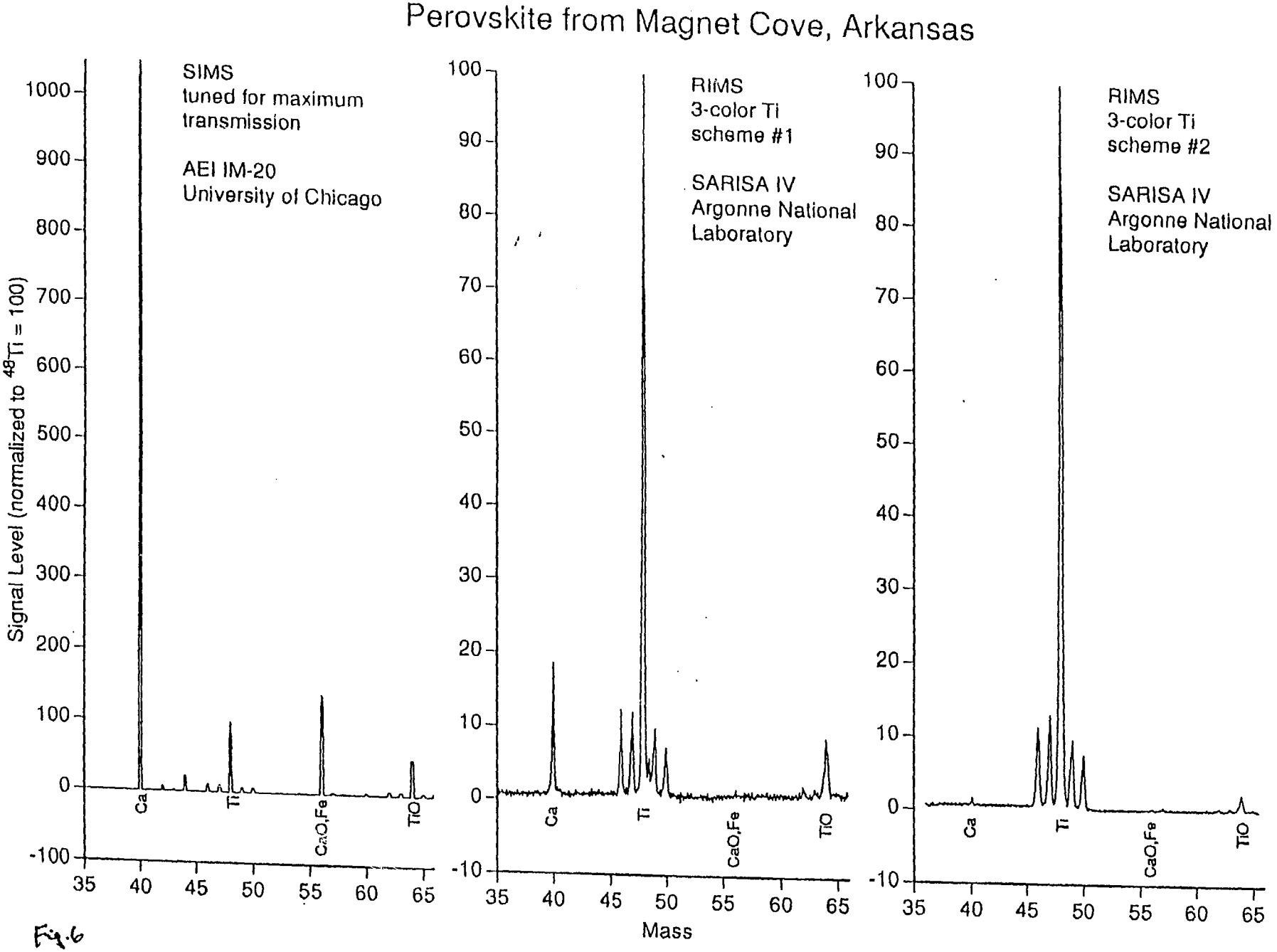
Perovskite from Magnet Cove, Arkansas
SIMS
tuned for maximum
transmission
AEI IM-20
University of Chicago
RIMS
3-color Ti
scheme #1
SARISA IV
Argonne National
Laboratory
RIMS
3-color Ti
scheme #2
SARISA IV
Argonne National
Laboratory
Signal Level (normalized to ^{48}Ti = 100)
Mass
Ca
Ti
CaO,Fe
TiO

Fig.6

D. Gruen
8/3/90

Titanium Photoionization Schemes

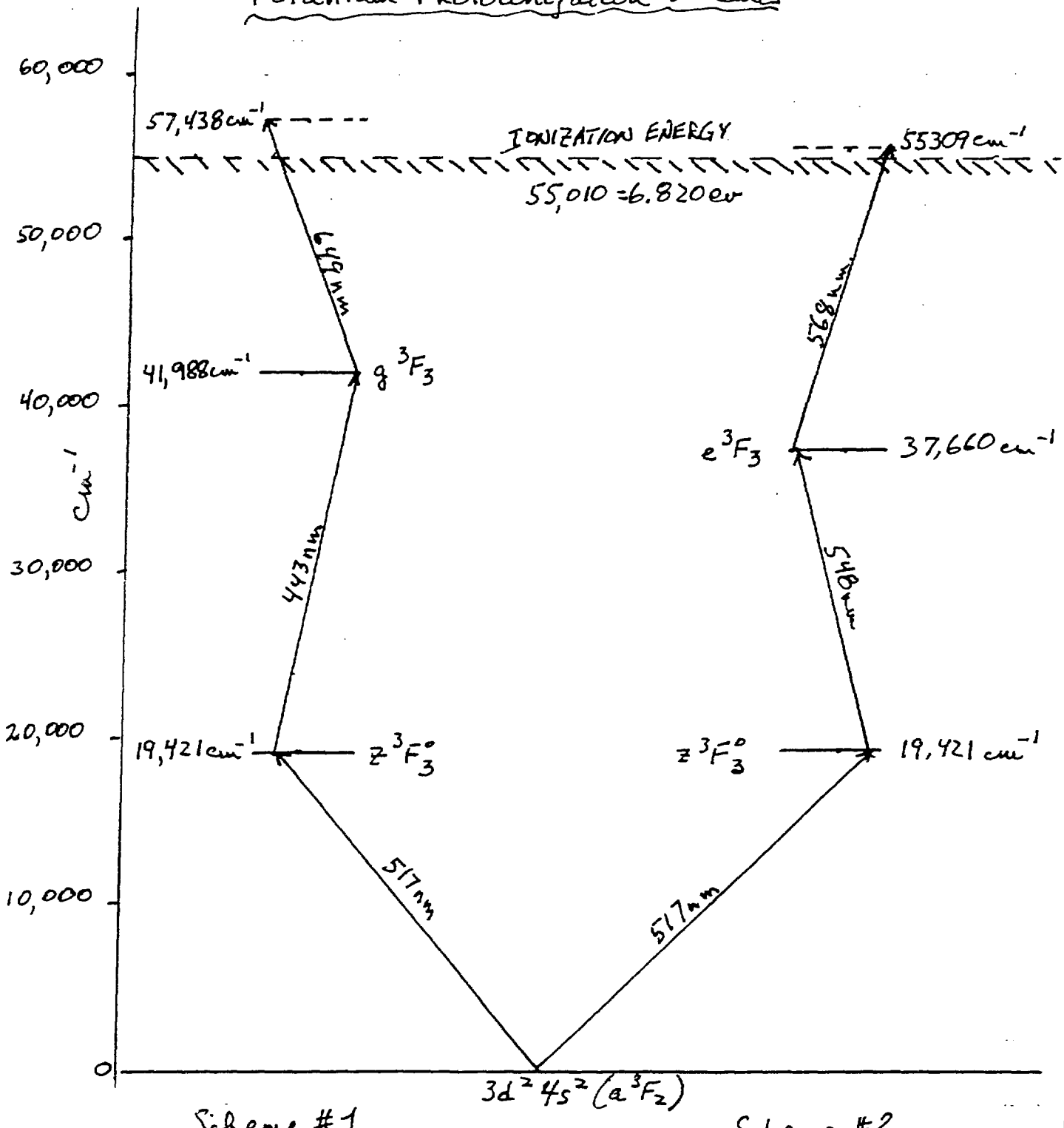

Fig. 7

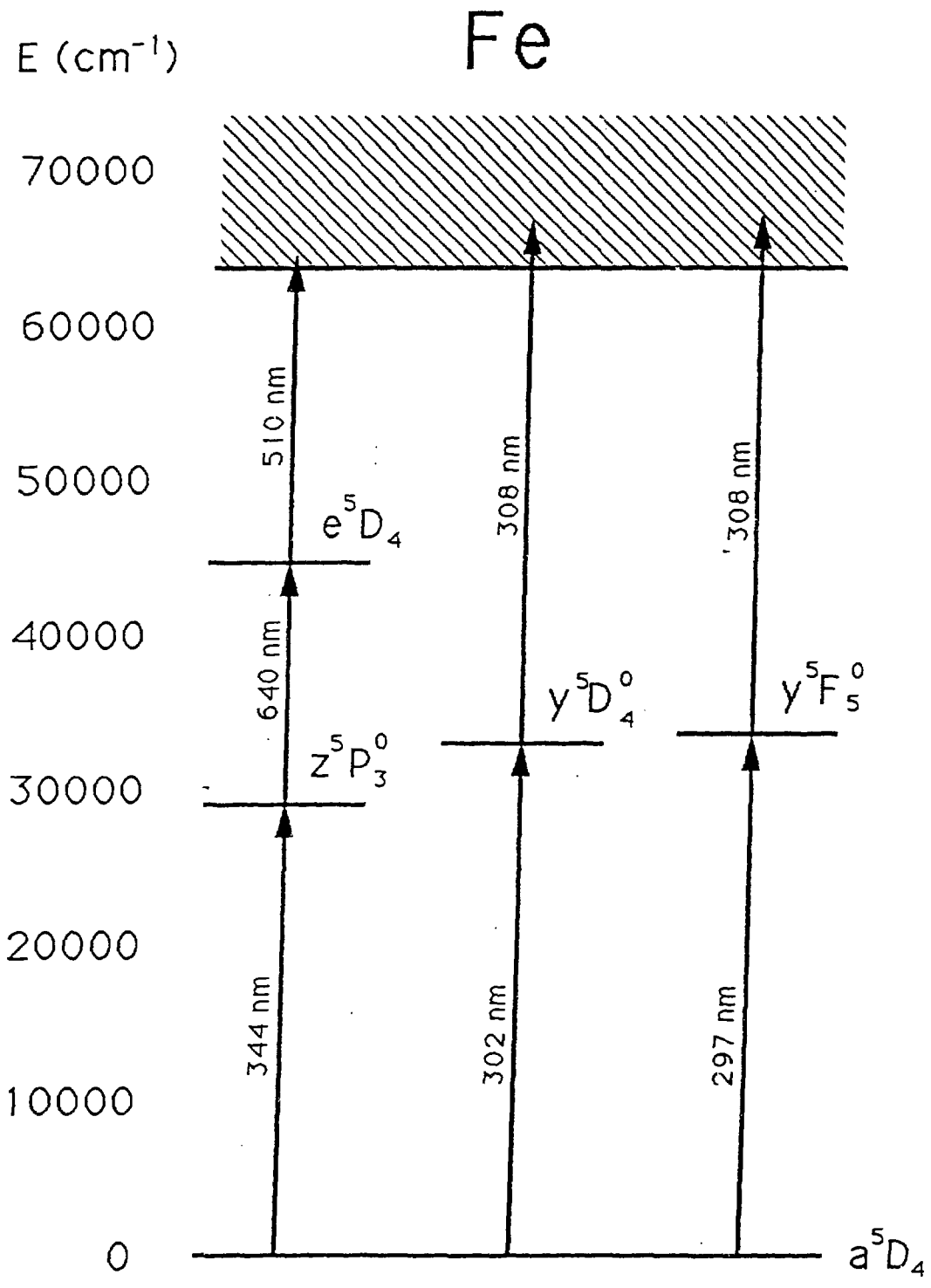
Fe
E (cm⁻¹)
70000
60000
50000
40000
30000
20000
10000
0
510 nm
640 nm
344 nm
308 nm
302 nm
308 nm
297 nm
e⁵D₄
z⁵P₃⁰
y⁵D₄⁰
y⁵F₅⁰
a⁵D₄

Fig. 8

Fe in Si Detection Limit for Two and Three Color RIS Schemes

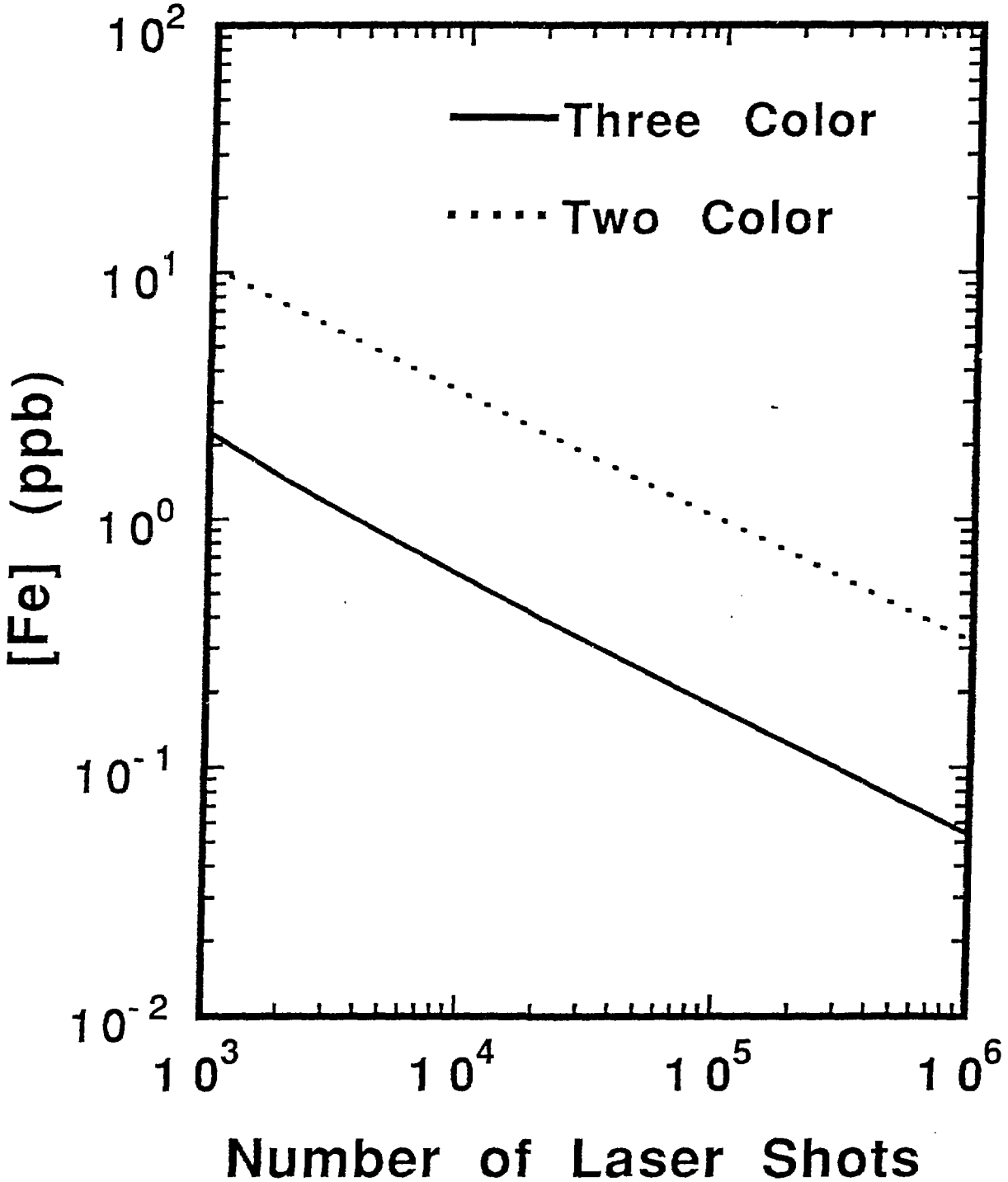

Fig. 9

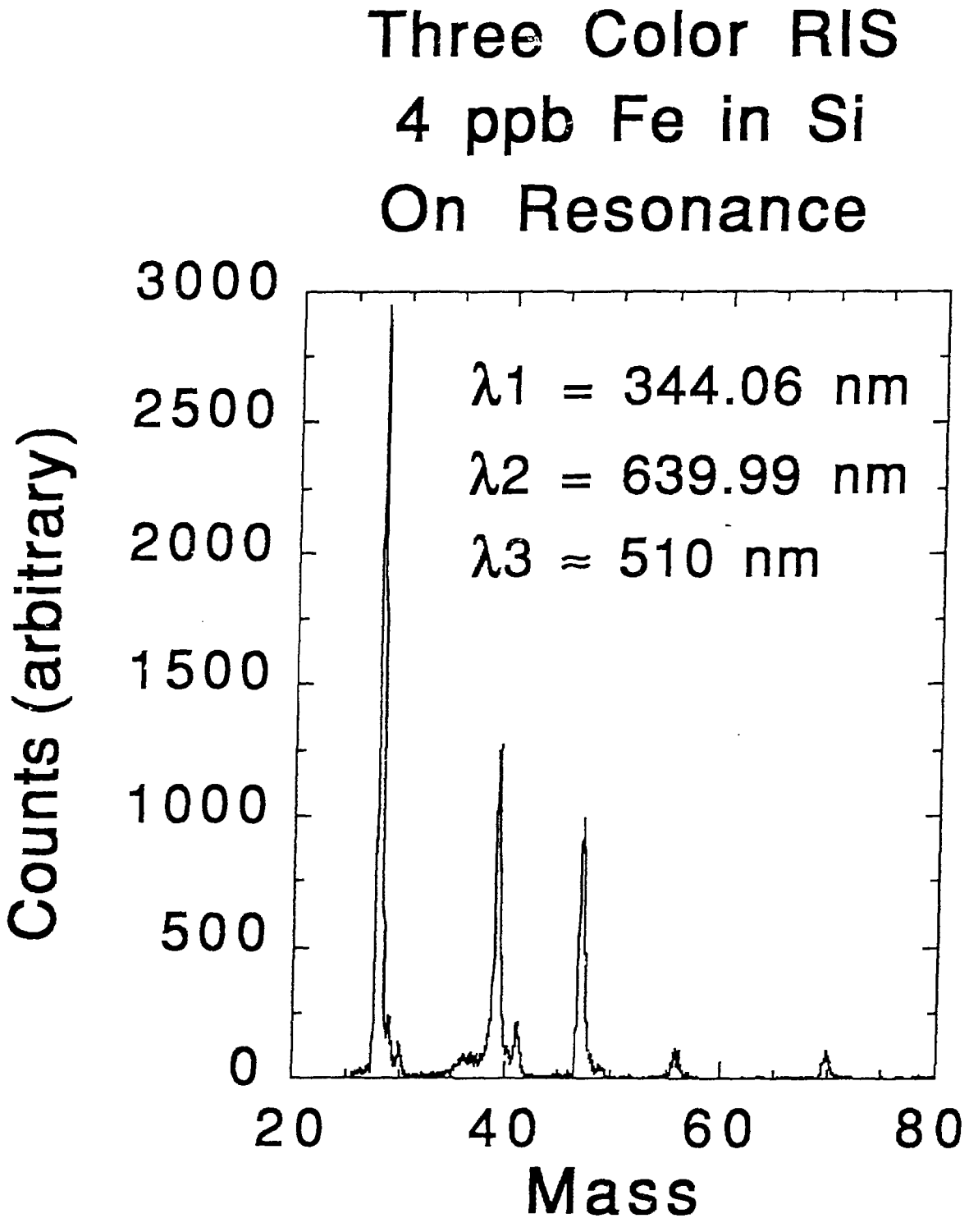
Three Color RIS
4 ppb Fe in Si
On Resonance
λ1 = 344.06 nm
λ2 = 639.99 nm
λ3 ≈ 510 nm
Counts (arbitrary)
3000
2500
2000
1500
1000
500
0
20
40
60
80
Mass

Fig. 10

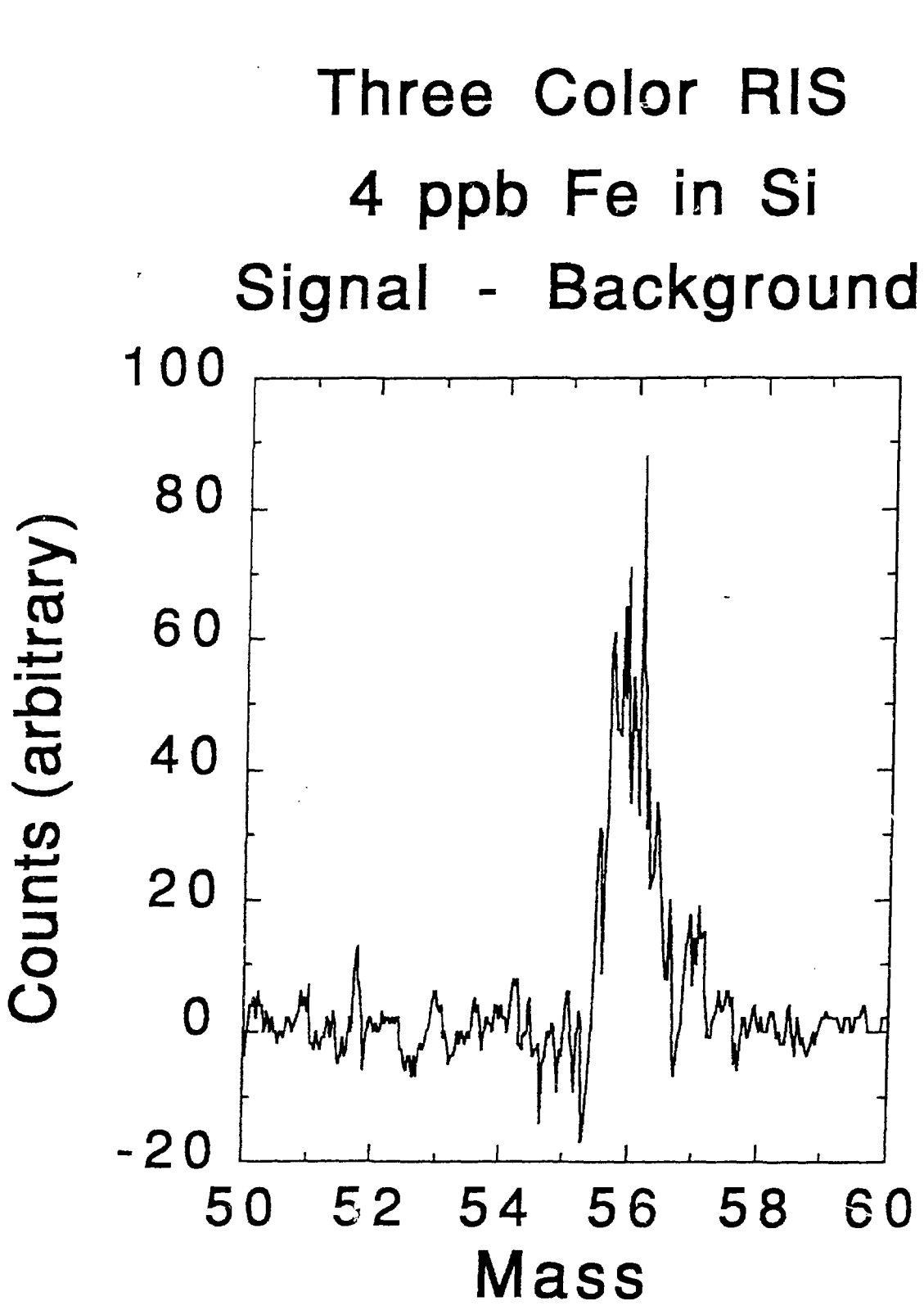
Three Color RIS
4 ppb Fe in Si
Signal - Background
Counts (arbitrary)
100
80
60
40
20
0
-20
50
52
54
56
58
60
Mass

Fig. 11

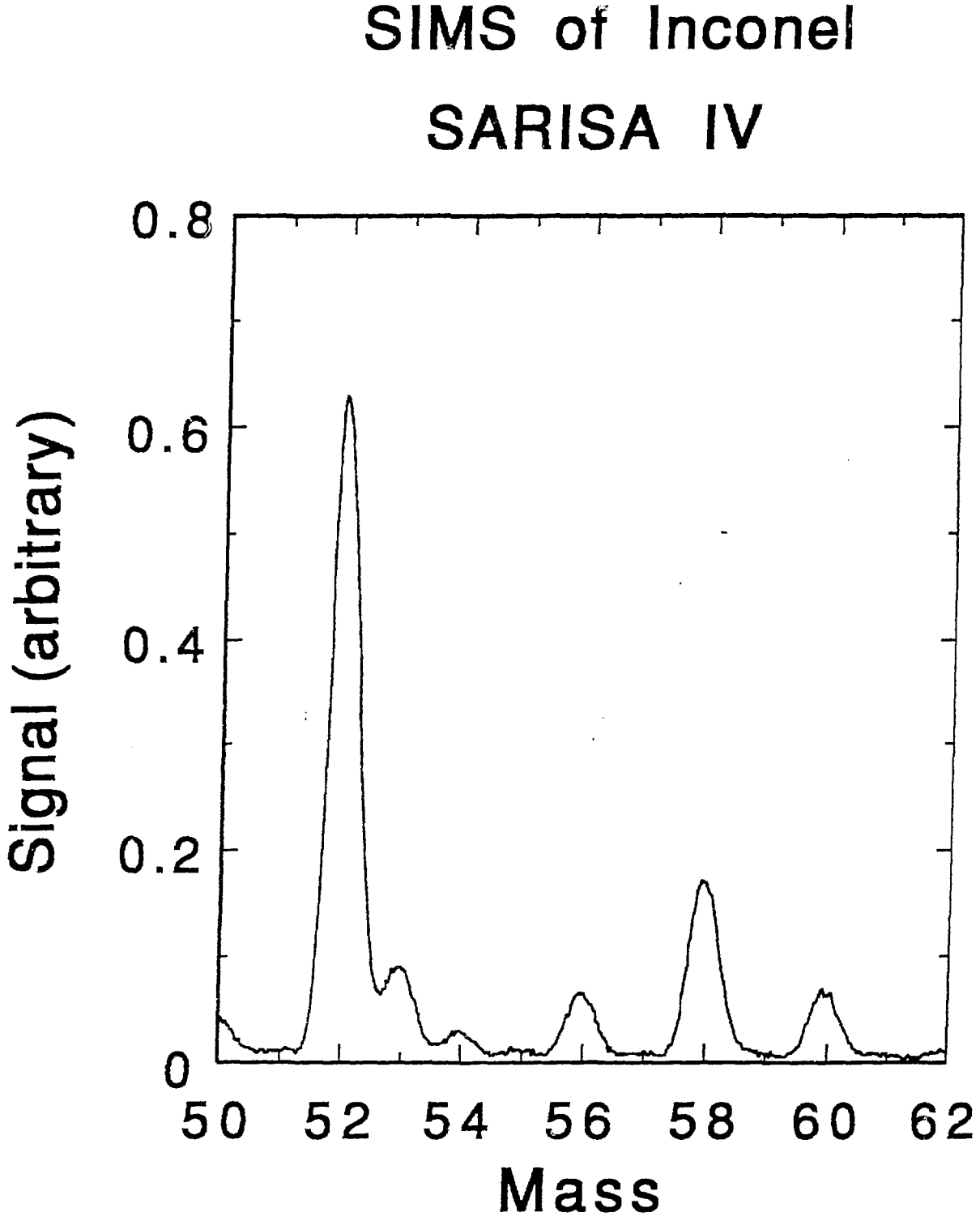
SIMS of Inconel
SARISA IV
Signal (arbitrary)
0.8
0.6
0.4
0.2
0
50
52
54
56
58
60
62
Mass

Fig. 12

Fe RIMS of Inconel On Resonance

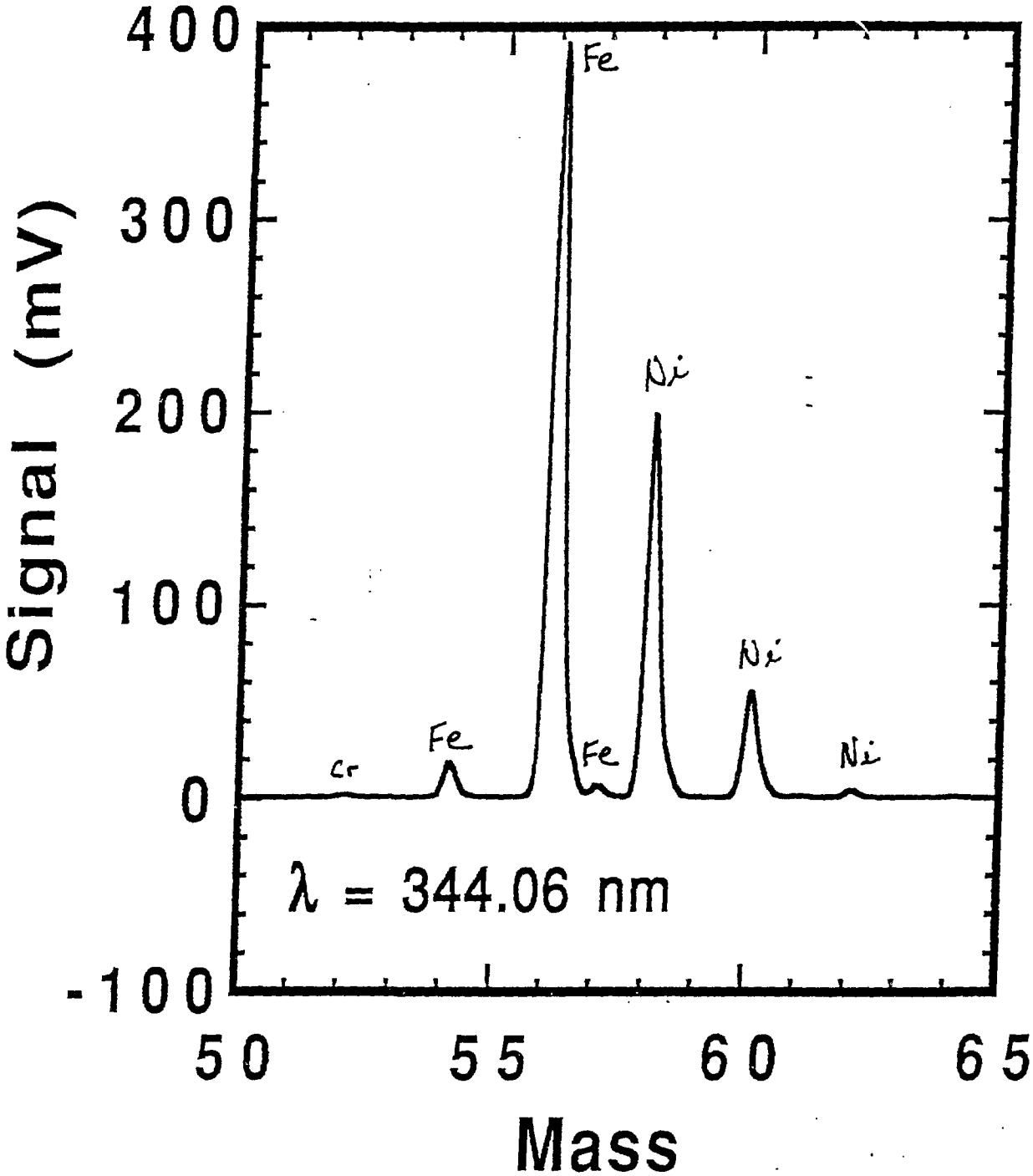

Fig. 13

Fe RIMS of Inconel Off Resonance

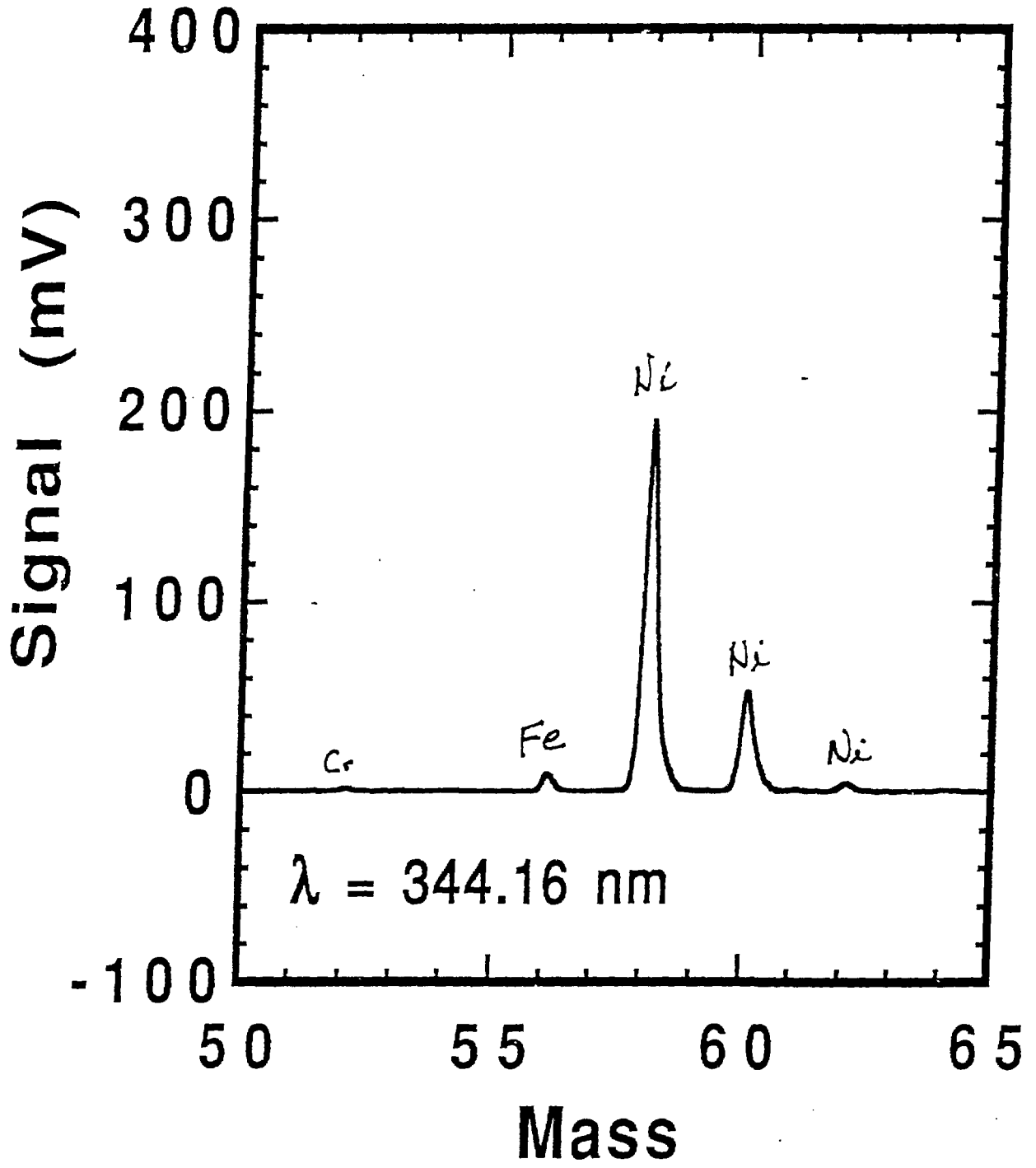

Fig. 14

Signal Enhancement for Multi-Colored RIS of Fe

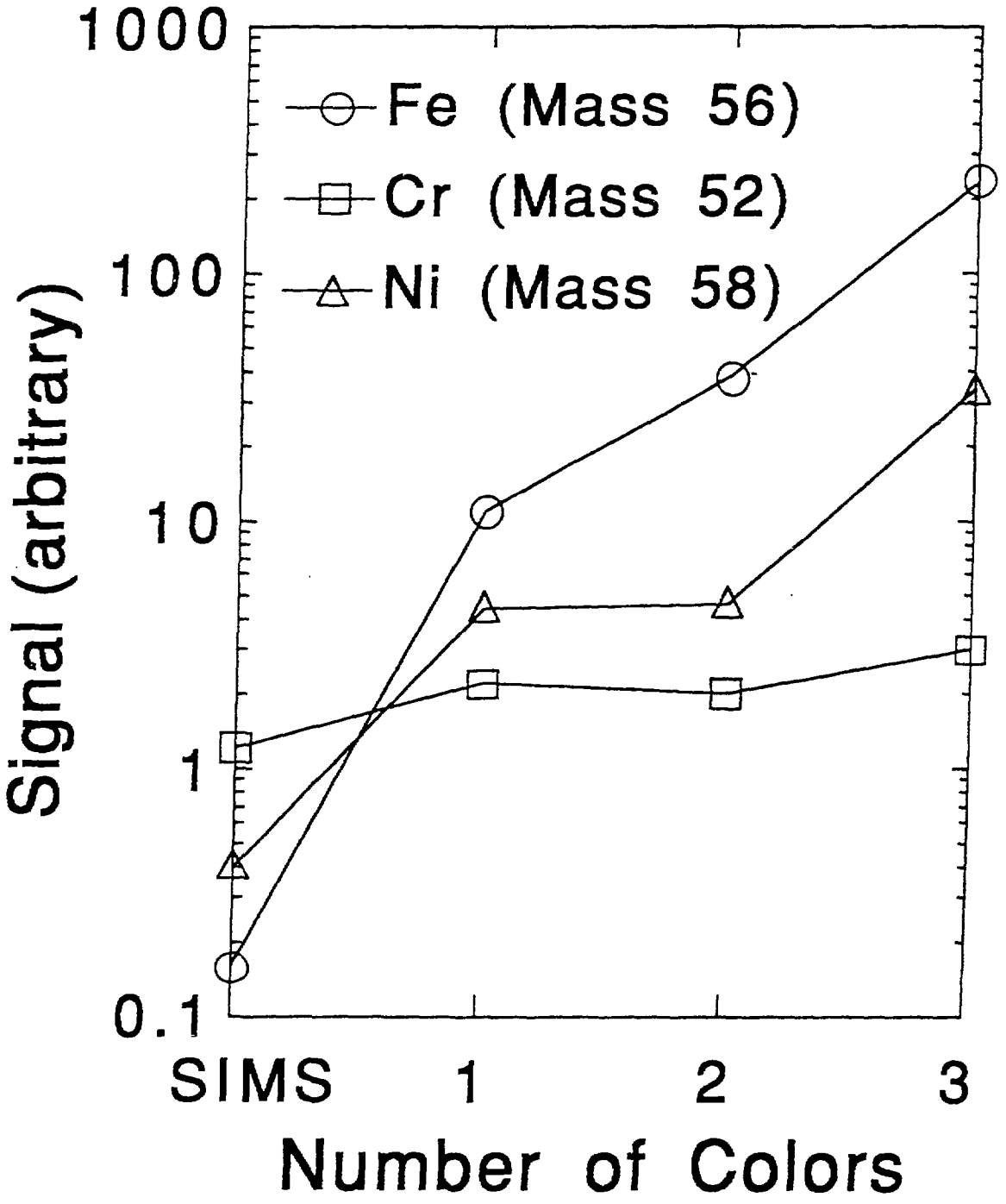

Fig. 15